Impact of river capture on erosion rates and offshore sedimentation revealed by geological and *in situ* ^{10}Be cosmogenic data (Corsica, western Mediterranean)

Marco G. Malusà[1*], Alberto Resentini[1], and Hella Wittmann[2]

[1] Department of Earth and Environmental Sciences, University of Milano-Bicocca, Piazza della Scienza 4, 20126 Milan, Italy
[2] Helmholtz Centre Potsdam, GFZ German Research Centre for Geosciences, Telegrafenberg, 14473 Potsdam, Germany

*Corresponding author: phone: +39 02 6448 2065; E-mail address: marco.malusa@unimib.it

Abstract. Quantitative analysis of fluvial topography and sediment yield changes are often independently used to detect major river capture events and episodes of drainage reorganization. Here we use a unique set of geological and *in situ* ^{10}Be cosmogenic data from Corsica, Western Mediterranean, to provide evidence of major river capture events affecting the former Paleo-Ostriconi river catchment during the Pliocene, and to illustrate how the landscape of Corsica is still reacting to the disequilibrium caused by the late Miocene uplift of Alpine Corsica. We found that ~1280 km^2 of basin area originally draining towards the Ligurian Sea were abruptly connected to the Tyrrhenian Sea by the capturing Tavignano and Golo rivers, which led to the formation of a large Pliocene-Quaternary submarine fan offshore the Tyrrhenian coast. The increased sediment yield towards the Tyrrhenian margin after river capture in the Pliocene was three times greater than the average sediment yield in the same source-to-sink system during the Holocene (410±100 t·km^{-2}·a^{-1} vs ~131±8 t·km^{-2}·a^{-1}) and greater magnitude than any subsequent peaks in sediment yield during late Pleistocene glaciations. ^{10}Be-derived denudation rates reveal that focused erosion still affects retreating knickpoints near the sites of former river capture in central Corsica, suggesting persistence of landscape disequilibrium for several millions of years. Our results demonstrate the potentially large impact of river capture on the stratigraphic record and highlight the importance of full consideration of landscape response times to onshore disturbances for any reliable interpretation of the offshore sedimentary archive.

Keywords: Paleo-Ostriconi river catchment; Pliocene river capture; provenance; source-to-sink analysis; long-lived knickpoints; Holocene erosion rates.

1. Introduction

An increasing number of source-to sink studies exploit the sedimentary archive to constrain landscape evolution and its response to tectonic and climatic forcing (e.g., Zheng et al., 2013; Bracciali et al., 2015; Castillo et al. 2017; Bender et al., 2020). Within this framework, sediment yield variations (e.g., Walford et al., 2005) and quantitative analysis of fluvial topography (e.g. Gallen, 2018; Loget and Van Den Driessche, 2009; Bowman, 2023) are often independently used to detect major river capture events and episodes of drainage re-organization (Shugar et al., 2017). The source-to-sink system of the Golo River, the largest catchment of Corsica (Western Mediterranean) provides a well-established test-case for this kind of studies. For example, Forzoni et al. (2015) and Molliex et al. (2021) analyzed the onshore part of the system during the late Quaternary climatic and sea level variations, whereas Calves et al. (2013) focused their attention on the offshore sink and highlighted major variations in sediment yield during the late Pleistocene and the last glacial cycle.

In this study, we expand the analysis of the river network of Corsica back to the Miocene, when Alpine Corsica was first exposed above sea level (e.g., Loÿe-Pilot et al. 2004; Malusà et al., 2015) (Fig. 1). We provide evidence of major river capture events affecting the former Paleo-Ostriconi River in the late Neogene, and we demonstrate that ~1280 km^2 of basin area originally draining towards the Ligurian Sea was abruptly connected to the Tyrrhenian Sea through headward erosion by the capturing Tavignano and Golo rivers. We document the impact of river piracy on offshore sedimentation and use a dataset of *in situ* ^{10}Be cosmogenic analysis on river sands to analyze the influence of disequilibrium inherited from river capture on pattern and rates of Holocene erosion. Our results illustrate the complex landscape response to tectonic uplift and provide a unique look at how a landscape reacts to external forcing on different time scales.

2. Geological setting

The island of Corsica is located in the Western Mediterranean (Fig. 1a), at the northern tip of the Corsica-Sardinia block, a continental fragment bounded by the Ligurian-Provençal basin to the west and the Tyrrhenian basin to the east (Rossi and Cocherie, 1991; Faccenna et al., 2001). Corsica emerges from the Mediterranean Sea with a typical wedge-shaped profile, showing elevations exceeding 2700 m a.s.l. in NW Corsica and gradually decreasing towards the SE (Fig. 1b, c). It mainly consists of Paleozoic rocks classically referred to as Variscan Corsica (e.g., Rossi et al., 2009), which are juxtaposed to the NE to the remnants of a Cenozoic subduction wedge formed during Alpine subduction and classically referred to as Alpine Corsica (e.g., Caron et al., 1990; Malusà et al., 2015) (Fig. 1d).

The Paleozoic magmatic rocks forming most of Variscan Corsica are encased into Panafrican units and Paleozoic high-grade metamorphic rocks (P′ and P in Fig. 1d) and belong to three different associations (U1 to U3 in Fig. 1d) (Rossi and Cocherie, 1991): U1 Mg–K plutonic rocks emplaced around 340 Ma and exclusively exposed in NW Corsica; U2 calc-alkaline plutonic rocks (e.g., monzonite, quartz-monzonite) emplaced around 320–290 Ma, and associated U2′ calc-alkaline volcanic rocks (e.g., andesite); and U3 alkaline and metaluminous magmatic rocks (e.g., Monte Cinto reddish rhyolite and vesiculated basalt) emplaced around 290 Ma. Sparse remnants of Mesozoic sedimentary successions are preserved along the Ostriconi Fault System (Fig. 1d), a major left-lateral tectonic structure parallel to the former Alpine subduction trench that remained active even after the late Eocene choking of Alpine subduction (Fig. 1a). Eocene to lower-Miocene conglomerates and Nummulitic flysch sequences (E2 and E3 in Fig. 1d) are either found unconformably on top of the Paleozoic units of Variscan Corsica, or partly accreted within the Cenozoic subduction wedge.

The Cenozoic subduction wedge of Alpine Corsica (A1-to-A3 in Fig. 1d) shares the same tectonic structure as the Western Alps, and it was originally part of the same, continuous orogenic segment (Fig. 1a). Its frontal part includes slivers of European continental crust, very-low-grade metaophiolites and flysch units (Balagne and Nebbio nappes) (A3 in Fig. 1d), and greenschist-to-blueschist facies metaophiolites and continental units (e.g., the Tenda unit, Rossetti et al., 2015) (A2 in Fig. 1d). The higher-pressure (>2 GPa) metaophiolites exposed on the Tyrrhenian side of Corsica (A1 in Fig. 1d) consist of calcschist, metagabbro and peridotite/serpentinite recording a late Eocene pressure peak and subsequent fast exhumation (dark blue in Fig. 1a) (Malusà et al., 2015).

Apenninic subduction started affecting the southern tip of the former Alpine subduction wedge by the end of the Oligocene (Fig. 1a), when Apenninic slab rollback started inducing extension in the Apenninic back arc leading to the opening of the Ligurian-Provençal basin in the early Miocene (Rollet et al., 2002), and of the Tyrrhenian basin in the late Miocene (Mauffret et al., 1999). In Alpine Corsica, back arc extension was associated with a trend of progressively younger AFT ages from the west to the east (Fig. 1f). AFT data in Variscan Corsica define instead a trend of northward decreasing ages (Fig. 1e, f) that mainly record the progressive northward translation of the Apenninic slab beneath the European plate during the Oligocene (Fig. 1a) (Malusà et al., 2016).

The Neogene uplift of Alpine Corsica above sea level is a first-order event in the landscape evolution of the region, probably triggered by the isostatic re-equilibration of the Corsica-Sardinia block after the opening of adjacent backarc basins (Malusà et al., 2016). Its age is constrained by the first appearance of clasts of high-pressure metaophiolitic rocks in the shallow-marine deposits of the Aleria Plain (N2 in Fig. 1d) (Loÿe-Pilot et al. 2004) and by the tilting of the Neogene strata exposed near St-Florent (N1 in Fig. 1d) (Rossi et al., 1994). Flat surfaces formed by marine abrasion are widespread in the landscape of Variscan Corsica (Danišík et al., 2012) (crosses in Fig. 1c). They are still preserved between the major incisions of the modern river network (Fig. 1b) and were not obliterated by the impact of Pleistocene glaciations, which only affected the highest part of the drainage divide (Kuhlemann et al. 2008) (Fig. 1c).

3. Methods

3.1 Geological and geomorphological analyses

Field geological and geomorphologic analyses were carried out within the framework of extensive 1/10.000-scale geological mapping performed by two of the authors (M.M. and A.R.) in northern Corsica between 2007 and 2019. We mapped marine terraces, raised beaches and river profile perturbations (e.g., knickpoints) and their relationships with the underlying geology over an area of ~1000 km^2. Our field observations were subsequently extended to the entire northern Corsica. We initially focussed our analysis to the beheaded Ostriconi Valley (Fig. 1b-d), carved along the Ostriconi Fault System and now occupied by a river evidently undersized compared to the size of the valley. We analyzed the modal composition of pebbles in Cenozoic conglomerates exposed within the Ostriconi drainage to detect potential changes in eroding sources and past supply of detritus from outside the modern Ostriconi catchment. This allowed us to reveal major river-capture events and infer the original extension of the newly defined Paleo-Ostriconi river catchment, and its progressive seizure through time.

Our field observations were cast within a more general framework provided by GIS-based geomorphological analysis, including knickpoint identification and chi-map creation using a digital elevation model with 30m spatial resolution (ASTER GDEM) and the TopoToolbox2 Matlab software (Schwanghart and Scherler, 2014). Stream network was extracted after DEM carving using a minimum upslope area of 0.45 km^2 (Fig. S1). Knickpoint identification was performed according to the quantile carving approach of Schwanghart and Scherler (2017). A chi map of the study area was created using a concavity m/n = 0.48 for the stream power incision model as derived from the Taravo River in southern Corsica, which was assumed to be in equilibrium (e.g., Perron and Royden, 2012). Chi analysis integrates the stream power equation from the outlet of the river to any given point along the river channel, originating a parameter of flow length normalized for drainage area that can be used as a proxy of the state of equilibrium of the river network.

To constrain the age of detected river capture events, we extended our modal compositional analysis to the Cenozoic conglomerates exposed outside the Ostriconi river catchment, based on an extensive compilation of literature data (Jauzein et al., 1976; Caron et al., 1990; Cubells et al., 1994; Ferrandini et al., 1999; Lahondère et al., 1994; Rossi et al., 1994; Loÿe-Pilot et al., 2004; Serrano et al., 2013; Molliex et al., 2021) validated by original observations. We finally analyzed the offshore sink using seismic reflection lines from the literature (LISA01, Contrucci et al., 2011; LISA10-W, Mauffret et al., 1999; BS97-22, Thinon et al., 2016; Calcagno et al., 2004) and estimated the volume of sediment accumulated in the Tyrrhenian Sea after the detected river-capture events. For time-to-depth conversion, we used a seismic velocity of 2.0 km s^{-1} for the Plio-Quaternary strata and 4.4 km s^{-1} for the Miocene strata (e.g., Contrucci et al., 2001; Thinon et al., 2016). Estimated Plio-Quaternary sediment volumes were converted into sediment yield by assuming a range of sediment densities between 1.4 $t \cdot m^{-3}$ (loosely packed sediment) and 2.3 $t \cdot m^{-3}$ (strongly packed sediment) to consider the impact of sediment porosity (e.g., Manger, 1963).

3.2 In situ ^{10}Be cosmogenic analysis

We collected six samples of modern river sands from the Ostriconi, upper Golo and Tartagine (S. Maria tributary) catchments for *in situ* ^{10}Be cosmogenic analysis to constrain the pattern and rates of Holocene erosion. The sampling strategy was conceived to obtain the highest number of nested sub-basins and sub-catchments (Granger et al., 1996) taking advantage of the samples previously analyzed by Molliex et al. (2017). We processed samples for *in situ* ^{10}Be separation in the *HELGES* laboratory, GFZ Potsdam, using the revised methods of von Blanckenburg et al. (2004) (see Supplementary material for analytical details). ^{10}Be/^{9}Be ratios were measured at the AMS at the University of Cologne (Dewald et al., 2013). To derive denudation rates, we calculated nuclide production using the CRONUS-Earth online calculator version 2.3 and the time-dependent scaling scheme of Lal/Stone (Lm) (Lal, 1991; Balco et al., 2008). Calculation of basin-wide ^{10}Be production rates (P_{total}, at·g^{-1}·a^{-1}) was carried out for each pixel in a 90 m digital elevation model (DEM), including a correction for topographic shielding (Dunne et al., 1999) that did not result in changes of more than 2% on production rates and was hence considered negligible. The absorption depth scale, which is the vertical distance over which the cosmic-ray flux decreases over the *e*-folding length, divided by the denudation rate gives the integration timescale of the method (von Blanckenburg, 2005). Effective denudation rates within nested catchments were computed following the approach of Granger et al. (1996). Results were compared with published denudation rates from ^{10}Be concentrations in granites from high-elevation paleosurfaces (Kuhlemann et al., 2008) and converted into a ^{10}Be-based sediment yield for an easier comparison with the sediment yield resulting from the analysis of the sedimentary record (e.g., Calves et al., 2013).

4. Results

4.1. Marine vs fluvial landforms

Our field data reveals that flat surfaces related to marine abrasion (e.g., Fig. 2a) are widespread not only in Variscan Corsica, as shown by previous studies (e.g., Danišík et al., 2012), but also in Alpine Corsica. They are carved in Tenda Unit metagranitoids and metasediments at elevations as high as ~ 400 m a.s.l. in the Agriates Desert (Fig. 2b), and as high as 1000 m a.s.l. on the right slope of the Ostriconi Valley, where they display an evident stepped configuration (Fig. 2d). Marine terraces of Alpine Corsica are locally covered by well-sorted sandstones with typical swash cross stratification that represent remnants of raised beaches. These sandstones are preserved at ~40 m a.s.l. near Punta di l'Acciolu (lat N 42.6912, long E 9.0681) (Fig. 2c), and at elevations as high as 95 m farther south near Monticellacciu (lat N 42.6709, long E 9.0848). Marine terraces detected in Alpine Corsica are distributed through an elevation range that is far beyond the range of eustatic sea level oscillations. They cut the regional foliation of Alpine metamorphic rocks and are thus demonstrably younger than Alpine metamorphism. Therefore, they are a useful marker to analyze the Neogene evolution of the island.

Field evidence reveal that, during Neogene uplift of Alpine and Variscan Corsica these marine landforms were progressively overprinted by fluvial landforms related to a nascent river network (Fig. 1b), which was in turn conditioned by the presence of major faults in the underlying basement. The Ostriconi Valley (Fig. 3a) is carved just along the Ostriconi Fault System (Fig. 1d), which juxtaposes the very-low-grade metaophiolites and metasedimentary rocks of the Balagne Nappe to the west (A3 in Fig. 1d) and the metagranitoids and paragneisses of the Tenda Unit to the east (A2 in Fig. 1d). The valley shows a smooth concave longitudinal profile (brown in Fig. 4a) and a transverse profile that is evidently too large to be related to the modern Ostriconi River (6 in Fig. 4b). The Ostriconi Valley is beheaded (Fig. 3a), and its original catchment area likely included regions located to the south of the Pietralba Pass (lat N 42.5392, long E 9.1841).

4.2. Modal compositions of Paleo-Ostriconi deposits

The mouth of the modern Ostriconi River (Fig. 5a) is characterized by fine-grained sediments typical of low-energy depositional environments, with no input of coarse detritus to the sea even during major floods. Nevertheless, we detected outcrops of ancient coarse-grained fluvial and fan-delta deposits near the Ostriconi river mouth. One of these outcrops is found in the Punta di Paraghiola locality (lat N 42.6673, long E 9.0590), where former fan-delta deposits are partly reworked to form a pebbly beach (Fig. 5e) (lat N 42.6717, long E 9.0605). Cobbles include metagranitoids of the Tenda Unit (Fig. 5f) and very-low-grade metasedimentary rocks of the Balagne Nappe, which form the metamorphic substratum of the river drainage, as well as rocks not exposed today in the modern Ostriconi river catchment, such as high-pressure metaophiolites (metagabbro, greenschist, serpentinite and other ultramafic rocks; Fig. 5g-k) and U2-U3 magmatic rocks (vesiculated basalt, vesiculated andesite with plagioclase phenocrysts, monzonite with K-feldspar phenocrysts, quartz-monzonite and Monte Cinto reddish rhyolite) (Fig. 5l-o). These deposits will be referred to as "Paleo-Ostriconi 1" stage hereafter (Fig. 6a). They attest to that the Ostriconi river drainage was much larger than today. The pie chart in Fig. 6a shows that cobbles derived from high-pressure metaophiolites (a=56.2%) and Alpine continental metamorphic rocks (b=28.5%) are dominant with respect to cobbles derived from Variscan rocks (c=14.6%) and the Balagne Nappe (d=0.7%) (see Supplementary Tables 1-2 for further details on modal composition of Paleo-Ostriconi detritus). Other remnants of reworked Paleo-Ostriconi 1 deposits are found east of Punta di l'Acciolu, where the pebbly beach of Cala di a Recisa (lat N 42.6917, long E 9.0685), near the eastern boundary of the Ostriconi Fault System, includes cobbles of serpentinite, greenschist, reddish rhyolite and metagranite.

Another relevant outcrop of ancient coarse-grained fluvial deposits preserved within the modern Ostriconi river drainage is found in the Ogliastro locality (lat N 42.6512, long E 9.0810) (Fig. 5c). It includes not only cobbles of metagranitoids and paragneisses of the Tenda Unit and metasediments of the Balagne Nappe, which form the metamorphic substratum of the modern Ostriconi river drainage, but also cobbles of quartz-monzonite (Fig. 5d), andesite with plagioclase phenocrysts, and Monte Cinto rhyolite (marked by arrows in Fig. 5c) that are not exposed today in the modern Ostriconi river catchment. These deposits will be referred to as "Paleo-Ostriconi 2" stage hereafter (Fig. 6a). Unlike the Anse de Peraiola deposits, they do not include cobbles of high-pressure metaophiolites. Cobbles of metagranitoids and paragneisses of the Tenda Unit are dominant (b=88%) compared to cobbles derived from Variscan Corsica (c=10%) and the Balagne Nappe (d=2%). Cobbles of Monte Cinto rhyolite are systematically smaller in size than the associated cobbles of plutonic rocks (Fig. 5c), as also observed in the modern fluvial deposits of the upper Golo valley, which are exclusively derived from erosion of Variscan rocks (Fig. 5b). Smaller remnants of Paleo-Ostriconi 2 deposits, with boulders of quartz-monzonite and reddish rhyolite, are recognized in the modern Ostriconi river catchment at elevations as high as 110 m a.s.l. near Monticellacciu (lat N 42.6703, long E 9.0843) and Cima Forca (lat N 42.6624, long E 9.0810), respectively. Notably, deposits with mixed Alpine-Variscan composition characterize not only the coarse-grained deposits of the Paleo-Ostriconi stages 1 and 2, but also the Pleistocene-Holocene successions exposed on the eastern coast of the island, as will be described in section 4.4. (Fig. 7).

4.3. Distribution of river knickpoints

The upper Golo valley is wide and relatively flat (Figs. 3b and 4b). It shows a major knickpoint and steepened valley walls downstream of the Calacuccia artificial lake (Fig. 3b-c). The knickpoint (lat N 42.3438, long E 9.0480) is indicated by a red square in Fig. 4a and is far from the main divide. Lithologies are the same before and after the knickpoint, consisting of Paleozoic magmatic rocks (Fig. 1d). Notably, there are other three rivers flowing towards the Tyrrhenian Sea that also show major knickpoints away from the main divide. They are the Asco River in the north and the Restonica and Tavignano rivers in the south (Fig. 4a). Rivers flowing towards the Ligurian Sea (e.g., Porto and Fango) are carved in the same lithologies as the upper Golo, upper Tavignano, Asco and Restonica, and often show steep walls cutting old planation surfaces (Fig. 3d). However, they do not show any major knickpoint away from the main divide, as instead observed in some of the rivers flowing towards the Tyrrhenian Sea (Fig. 4a). A systematic analysis of transverse valley profiles reveals that the Ostriconi and the upper and intermediate Golo valleys are much wider than the lower segments of the Golo and Tavignano valleys (Fig. 4b). Chi analysis shows that the upper and intermediate segments of the Golo and Tavignano catchments have higher chi values (>$5 \cdot 10^3$) than the nearby catchments (Fig. 8c), supportive of a transient landscape with the drainage divide moving toward higher-chi headwaters.

4.4. Modal composition of conglomerates outside the Ostriconi River drainage

The sparse Eocene to mid-Miocene conglomerates preserved in northern and central Corsica have modal compositions invariably pointing to clastic sources located in Variscan Corsica or in the frontal part of the Cenozoic subduction wedge (e.g., Rossi et al., 1994; Ferrandini et al., 1999; Loye-Pilot et al., 2004). The Eocene conglomeratic successions of Palasca and Lozari and the Oligocene Vazzio conglomerate preserved on top of the Variscan basement (1 to 3 in Fig. 7) chiefly consist of cobbles of Paleozoic volcanic and plutonic rocks. The Eocene succession of Punta di l'Acciolu (4 in in Fig. 7), lying on top of the Tenda Unit, includes cobbles derived from the Tenda Unit, the Balagne Nappe and Variscan Corsica, but no clasts of high-pressure metaophiolites (Rossi et al., 1994). The ~600 m thick Burdigalian - lower Tortonian succession exposed near Francardo-Ponte Leccia (5 in Fig. 7) consists of continental conglomerates chiefly including Variscan rock cobbles (Ortone and Francardo formations) and, in between, Burdigalian lagoonal to shallow marine deposits with cobbles of Variscan rhyolite (Taverna Formation) (Cubells et al. 1994). The ~400 m thick Miocene succession exposed near St-Florent (6 in Fig. 7) consists of: (i) basal continental conglomerates (Fium Albino Formation) with cobbles of Tenda Unit metagranitoids; (ii) mid-Burdigalian to lower Langhian calcarenites (Sant'Angelo Formation) with rhodoliths grown around clasts derived from the underlying Nebbio Nappe, the Tenda Unit and Variscan Corsica, and Monte Cinto rhyolite clasts that become dominant up section in the St Florent conglomerate; (iii) upper Langhian - lower Serravallian marls and calcarenites (Farinole Formation) with channelized conglomerate bodies mainly including Monte Cinto rhyolite cobbles (Rossi et al., 1994).

A similar picture is provided by the ~2 km thick stratigraphic succession exposed in the Aleria Plain, which is almost complete from the Burdigalian to the Messinian (Fig. 7). Until the early Tortonian, detritus in the Aleria Plain was exclusively supplied from erosion of Variscan Corsica (Loye-Pilot et al., 2004; Serrano et al., 2013): (i) the mid-Burdigalian Saint-Antoine Formation includes (sandy) marls and massive breccia with blocks of greenish granite; (ii) the Langhian marls and conglomerates of the Aghione Formation include cobbles of Variscan rhyolite and granite; (iii) the Serravallian Alzitone Formation consists of pebbly sandstones with cobbles of greenish granite;

(iv) the lower Tortonian Vadina Formation consists of marine sedimentary rocks with interleaved sandstone and conglomerate containing clasts of Variscan rhyolite and granite.

On the eastern coast of the island, the first appearance of detritus derived from high-pressure metaophiolites is recorded in the upper Tortonian Casabianda Formation (Fig. 7) (Loÿe-Pilot et al. 2004). Later on, high-pressure metaophiolites provided most of the detritus supplied to the lower Messinian Aleria Formation, including cobbles of calcschist, greenschist, metachert, metagabbro, peridotite, and to a lesser extent Variscan granites and rhyolites. A mixed Alpine-Variscan provenance characterizes all the Quaternary deposits of the Tavignano river terraces (Fz2-Fv in Fig. 7), which contain cobbles of Variscan granite and rhyolite beside cobbles of high-pressure calcschist, metagabbro and peridotite. By contrast, no Variscan rock cobble is observed in the Plio-Quaternary formations of the Costa Verde (Fig. 7), where the upper Pliocene Peri Formation exclusively contains cobbles of high-pressure metaophiolitic rocks, and the Quaternary deposits of the Bravona river terraces show a pure Alpine provenance with cobbles of high-pressure calcschist, metagabbro, greenschist and glaucophanite (Fz2-Fv in Fig. 7) (Jauzein et al., 1976; Caron et al., 1990).

Farther north, the uppermost Miocene – Pliocene Casatora Formation exclusively contains clasts of high-pressure calcschist, greenschist and quartz (Lahondère et al., 1994). In the Marana Plain, the first evidence of mixed Alpine-Variscan composition is provided by the ~2.6 Ma old conglomerate from the GBEC5 borehole (Molliex et al., 2021). Mixed Alpine-Variscan compositions are also invariably observed in the Quaternary deposits of the lower Golo river terraces (Fz to Fv in Fig. 7).

4.5. In situ ^{10}Be cosmogenic data

In situ ^{10}Be concentrations measured in samples S1 to S6 range from 10.24±0.49 to 17.75±0.78 $\times 10^4$ at·g_{QTZ}^{-1} (Table 1). ^{10}Be-derived denudation rates are between 67.6±4.1 mm·ka^{-1} in the uppermost Golo (sample S1) and 37.2±2.4 mm·ka^{-1} near the mouth of the Ostriconi River (sample S6). Associated apparent ages range from 12.2 ka (sample S1) to 23.8 ka (sample S6).

When these data are combined with previous data by Molliex et al. (2017), the effective denudation rates computed for nested catchments provide a finer image of the Holocene erosion pattern in northern Corsica (Fig. 8b and Supplementary Table 3). In the Ostriconi River catchment, ^{10}Be-derived denudation rates decrease downstream, as normally expected for a river in equilibrium, from ~43 to ~32 mm·ka^{-1}. ^{10}Be-derived denudation rates are ~30-33 mm·ka^{-1} in the Lagani and Tartagine catchments, and ~49-52 mm·ka^{-1} in most of the Asco and upper Golo catchments, where denudation rates are as low as ~15 mm·ka^{-1} near the main drainage divide.

Rates ~47 mm·ka^{-1} are observed in the Restonica Valley, and rates ~74 mm·ka^{-1} are found in the upper Tavignano Valley. These values are systematically higher than the ^{10}Be-derived denudation rates, between ~9 and ~24 mm·ka^{-1}, measured in granites from high-elevation paleosurfaces (Kuhlemann et al., 2008) (Fig. 8b).

A downstream increase in denudation rates, from ~62 to ~95 mm·ka^{-1}, is observed along the Casaluna catchment. The highest denudation rates (>200 mm·ka^{-1}) are found in central Corsica, in river segments located along the Ostriconi Fault System (Fig. 8b), such as along the intermediate Golo Valley to the south of the Pietralba Pass (Fig. 3a). Denudation rates drop sharply in the lower Golo Valley, where they are much lower (<4 mm·ka^{-1}) than in the nearby catchments draining towards the Tyrrhenian Sea (Bevinco, Fium Alto and Bravona in Fig. 8b). If similar denudation rates <4 mm·ka^{-1} are considered for the lower Tavignano river segment, denudation rates would exceed 200 mm·ka^{-1} also in the intermediate Tavignano Valley, to the south of the San Quilico Pass (Fig. 3e). *In situ* ^{10}Be concentrations measured in the Golo and Tavignano catchments can be converted into an average Holocene ^{10}Be-based sediment yield of ~131±8 t·km^{-2}·a^{-1} (Supplementary Table 4).

4.6. Sediment volume in the offshore sinks

Seismic lines LISA01 and LISA10-W reveal that the thickness of the depositional sequences, from the base Langhian to the base of Messinian salinity crisis (MSC) deposits, is greater in the Ligurian Sea offshore the Ostriconi river mouth compared to the Tyrrhenian Sea offshore the Golo and Tavignano river mouths (~3.1 vs. ~2.4 km, respectively, in grey in Fig. 9a). By contrast, the Pliocene-Quaternary isopachs (in red in Fig. 9a) indicate much thicker Pliocene-Quaternary deposits offshore the Tyrrhenian side of the island (Calcagno et al., 2004; Thinon et al., 2016) compared to the Ligurian side (>1.0 km vs. ~0.4 km). The Pliocene-Quaternary deposits offshore the Tyrrhenian side define a coalescing fan shape geometry, which is evident both in map view (Fig. 9a) and in cross section (Fig. 9c). Seismic reflectors are weaker in the lower part of the fan and more evident in the upper part, where the typical architectures of a small turbidite system are described in detail by previous work (e.g., Gervais et al., 2004; Sømme et al., 2011; Sweet et al., 2020; Calves et al., 2013). The apex of the fan is in the region between the Golo and Tavignano river mouths, and the Pliocene-Quaternary depocenter is evidently shifted northwards compared to the underlying and much thinner MSC deposits (Fig. 9a). Based on these observations, the volume estimate of these Pliocene-Quaternary fan deposits (~2.1×10^{12} m^{3}), which are evidently sourced from Corsica, can be used to evaluate an average Pliocene-Quaternary sediment yield from the Golo and Tavignano catchments, which is equal to ~410±100 $t \cdot km^{-2} \cdot a^{-1}$ (Supplementary Table 4).

5. Discussion

5.1. Drainage evolution and river capture events

The bedrock gorges of central Corsica testify to a rapid base-level drop in the drainage network of the island (Fig. 3b-d). The presence of major knickpoints along the longitudinal profiles of the Restonica, Tavignano, upper Golo and Asco rivers, all flowing towards the Tyrrhenian Sea, and the absence of major knickpoints away from the main divide in rivers flowing towards the Ligurian Sea (Fig. 4a), cannot be explained exclusively with an overincision due to a relative lowering of sea level linked to eustatic causes or to the tectonic uplift of the entire island (e.g., Malusà et al., 2016). Instead, they also require a transient response of the drainage network to a more localized lowering of the base level due to river capture, resulting in reorganization of the river network.

The morphology of the modern Ostriconi Valley, which is carved along the NNW-SSE Ostriconi Fault, and the provenance of associated river gravels provide additional evidence of a major river capture. The Ostriconi Valley is clearly beheaded (Fig. 3a), which indicates that the upper part of the Ostriconi catchment was originally extended to the south of the Pietralba Pass, where chi analysis is also supportive of a transient landscape (Fig. 8c).

Clast lithologies in gravels of the Paleo-Ostriconi 1 stage (t_1 in Fig. 6a) are dominated by rocks not exposed today in the Ostriconi river catchment. They include a distinctive suite of metagabbro, greenschist, serpentinite and other ultramafics rocks (a=56.2% in Fig. 6a) that indicates sourcing from the high-pressure metaophiolites of the Castagniccia tectonic dome (Monte S. Petrone), which are exposed farther to the SE. A second distinctive suite of vesiculated basalt, vesiculated andesite with plagioclase phenocrysts, monzonite with K-feldspar phenocrysts, quartz-monzonite and Monte Cinto reddish rhyolite (c=14.6%) indicate instead sourcing from U2-U3 magmatic rocks of Variscan Corsica exposed farther to the SW. Such a range of clast lithologies allow for a detailed reconstruction of the Paleo-Ostriconi 1 catchment to the south of the Pietralba Pass, which likely included the upper and intermediate Golo and Tavignano, Tartagine, Asco, Restonica and Vecchio rivers, originally forming a dendritic pattern that can be recognized in map view even today (see Fig. S2). Figure 6b shows the modern river profiles rearranged according to their position in the inferred Paleo-Ostriconi 1 catchment and shows that transverse river profiles from outside the Paleo-Ostriconi 1 catchment (e.g., G5-6 and T3-4 in Fig. 6b) are invariably narrower and likely at a different stage of evolution. During the Paleo-Ostriconi 1 stage, the main watershed in northern Corsica was located much further east than today, i.e., in Alpine Corsica (Fig. 6a).

Clast lithologies in gravels of the Paleo-Ostriconi 2 stage (t_2 in Fig. 6a) reveal a first major change in drainage network. They include metagranitoids and paragneisses of the Tenda Unit (b=88% in Fig. 6a), very low-grade rocks of the Balagne Nappe (d=2%), and a suite of quartz-monzonite, andesite with plagioclase phenocrysts, and Monte Cinto rhyolite already observed during the Paleo-Ostriconi 1 stage (c=10%). However, no cobble of high-pressure metaophiolites is observed in the Paleo-Ostriconi 2 gravels. The disappearance of metaophiolitic clasts (56% of the total amount of clasts during the Paleo-Ostriconi 1 stage) is not attributable only to a sampling bias and indicates that part of the Paleo-Ostriconi 1 basin area was abruptly connected to the Tyrrhenian Sea by the capturing Tavignano River. Based on the reconstruction of Fig. 6b, we estimate that ~475 km^2 of basin area was diverted at that time. The elevation of the S. Quilico Pass (1 in Fig. 6a), located along the original Paleo-Ostriconi 1 valley floor, provides a lower-bound constraint to the amount of overincision from the time of river capture. It likely exceeded 400 m (Fig. 6b), pointing to an average erosion rate >200 $mm{\cdot}ka^{-1}$ in the past 5 Ma, which is consistent with the ^{10}Be-derived denudation rates documented during the Holocene near the capture site. During the Paleo-Ostriconi 2 stage, the Paleo-Ostriconi River was still able to convey coarse debris from the Monte Cinto caldera to the modern Ostriconi river mouth.

A second major episode of river piracy affecting the Paleo-Ostriconi basin was governed by the capturing Paleo-Golo River. This capture abruptly connected to the Tyrrhenian Sea ~805 km^2 of basin area chiefly including Variscan magmatic rocks and originally belonging to the Paleo-Ostriconi 2 catchment, leading to the river network configuration observed today (Fig. 6a). Since then, no supply of coarse debris from Variscan Corsica (c in Fig. 6a) has ever reached the mouth of the small (~65 km^2) and beheaded Ostriconi Valley (Fig. 5a), because that debris is funneled today into the narrow, V-shaped lower Golo Valley (G5 and G6 in Fig. 6b).

Alternative hypotheses to the proposed two-stage river capture evolution are not consistent with field data. A shorter Paleo-Ostriconi would not explain the occurrence of high-pressure metaophiolitic clasts in the Paleo-Ostriconi 1 deposits. A single-stage evolution would not explain the disappearance of the high-pressure metaophiolitic clasts when moving from the Paleo-Ostriconi 1 to the Paleo-Ostriconi 2 deposits. A two-stage evolution starting with the capture by the Paleo-Golo followed by the capture by the Paleo-Tavignano would not explain the presence of clasts of igneous rocks from Variscan Corsica in the absence of clasts of high-pressure metaophiolitic rocks in the Paleo-Ostriconi 2 deposits.

5.2 Age of river capture and impact on offshore sedimentation

The Paleo-Ostriconi 1 drainage network was necessarily established after the uplift and subaerial exposure of the high-pressure metaophiolites of Alpine Corsica. The age of this major geologic event is constrained to the late Tortonian by the first appearance of metaophiolitic debris in the Casabianda Formation (Aleria Plain, Fig. 7) (Loye-Pilot et al., 2004). The Tenda Unit and Variscan Corsica have long represented the exclusive source of detritus accumulated around Corsica, at least between the Eocene and the middle Miocene (Fig. 9), whereas in the late Tortonian metaophiolitic debris became overwhelming all along the eastern coast of the island (Fig. 7). The renewed appearance of Variscan rock cobbles in fluvial conglomerates exposed on the eastern coast of the island provides an upper bound constraint to the age of the Paleo-Golo river capture, which marks the end of the Paleo-Ostriconi 2 stage. These cobbles are found in the ~2.6 Ma old conglomerate ($^{26}Al/^{10}Be$ burial ages by Molliex et al., 2021) sampled in the GBEC5 borehole in the Marana Plain. Therefore, the two-stage river capture evolution illustrated in Fig. 6a can be bracketed between the late Tortonian and the Pliocene, which is also consistent with the lower bound constraints provided by AFT and AHe thermochronologic ages (Fig. 1e-f, Fig. 7). These thermochronologic ages were set before the drainage network was established. Overincision during and after river capture was not deep enough to reach the partial annealing/retention zones of the AFT and AHe thermochronologic systems, which implies that exhumation linked to river capture is not expected to be recorded by low-temperature thermochronometers in rocks exposed today in central Corsica.

Starting from the Pliocene, ~1280 km^2 of basin area originally draining towards the Ligurian Sea were thus abruptly connected to the Tyrrhenian Sea by the capturing Tavignano and Golo rivers. This event determined a shift of depocenter in the Tyrrhenian Sea (Fig. 9a) and the formation of a large Pliocene-Quaternary submarine fan offshore the region between the Golo and Tavignano river mouths. The volume of the fan (~2.1×10^{12} m^3) implies an average Pliocene-Quaternary sediment yield from the Golo and Tavignano catchments that is three times greater than the average Holocene sediment yield from the Golo and Tavignano based on *in situ* ^{10}Be

concentrations (410±100 t·km^{-2}·a^{-1} vs ~131±8 t·km^{-2}·a^{-1}). These findings indicate a higher sediment yield during the early stages of drainage reorganization.

5.3 Impact on pattern and rates of Holocene erosion

Although the diversion of the Paleo-Ostriconi river catchment to the Tyrrhenian Sea ended no later than ~ 2.6 Ma ago, the erosion pattern of central Corsica during the Holocene still reflects the Pliocene fluvial capture events, as illustrated by the reconstruction of the Paleo-Ostriconi river profile and associated ^{10}Be-derived denudation rates (Fig. 8d). ^{10}Be-derived denudation rates measured in modern river sands are systematically higher than the ^{10}Be-derived denudation rates measured in granites from high-elevation paleosurfaces. This suggests ongoing active erosion along the steep Corsican gorges that formed after capture-related base level lowering.

Given the age of river capture and the distance of knickpoint retreat (e.g., Bowman, 2023), we can infer that the upper Tavignano knickpoint migrated ~10 km in 5 Ma, at a rate of ~2 mm·a^{-1}. The upper Golo knickpoint migrated 8-9 km in 4 Ma, at a similar rate of ~2 mm·a^{-1}, with an upper bound of ~3.5 mm·a^{-1} defined by the 2.6 Ma ^{26}Al/^{10}Be burial age of the GBEC5-2 conglomerate. These values are consistent with previous studies on bedrock gorges (e.g., Weissel and Seidl, 1997; Loget and Van Den Driessche, 2009), and explain the highest denudation rates (~220 mm·ka^{-1}) provided by cosmogenic data along segments of the Ostriconi Fault System corresponding to previous capture sites (i.e., south of the Pietralba Pass and south of the S. Quilico Pass) (Fig 8b). These ^{10}Be-derived denudation rates are four-to-five times greater than Holocene average erosion rates measured along the river network (Fig 8b), and likely integrate a basin-wide average denudation rate with a much faster denudation rate characterizing the regions around the knickpoints. This demonstrates that the landscape is still responding to the disequilibrium caused by the uplift of Alpine Corsica, with focused erosion occurring at rates similar to the peak rates that affected the system during the late Pleistocene glaciations (~219 mm·ka^{-1}, Calves et al. 2013).

5.4 Influence of glaciers and lithology

Calves et al. (2013) highlighted an increase in sediment yield offshore the Golo during the last glacial cycle (blue boxes in Fig. 9b), which is anyway smaller than the peak in sediment yield triggered by the river capture events documented in this study. Glaciers in Corsica were exclusively developed on resistant Variscan rocks on the left slopes of the Paleo-Ostriconi drainage basin, with the Golo and Asco knickpoints located outside the main Wurmian glaciers, and the Tavignano and Restonica knickpoints located just at their boundaries (Fig. 1c). Detritus supply per unit area was systematically higher in the eastern side of the (Paleo)Ostriconi Valley, carved in less resistant high-pressure rocks (a and b in Fig. 6a) and hosting the largest alluvial fans (e.g., the Urtaca alluvial fan, Fig. 3a), compared to the glaciated western side of the valley mainly carved in more resistant Variscan rocks (c in Fig. 6a). This suggests a minor influence of the small Corsica glaciers compared to lithology, at least during the interglacial stages.

6. General implications

The unusually well documented basin history in Corsica provides a unique look at how a landscape reacts via multi-stage river capture to the perturbation caused by a major tectonic uplift event. It demonstrates that river captures are drivers of landscape modification with a potentially large impact on the stratigraphic record. However, a major change in sediment flux due to river piracy accommodating tectonic uplift can occur millions of years after the triggering tectonic event (3 Ma in Corsica). Although the sediment yield after river capture is generally much greater than the average sediment yield observed in the same source-to-sink system at a later stage of evolution, the concentration of erosion at long-lived knickpoints can be observed at even longer timescales after tectonic uplift (7-8 Ma in the Corsica case). Using the sedimentary archive to constrain the tectonic growth of topography thus requires that the different timescales of landscape response to tectonic perturbations are duly accounted for, with important implications for any source-to-sink study aimed at interpreting the stratigraphic record in terms of tectonic or climate variations.

7. Conclusions

Our study illustrates how the landscape of Corsica has reacted and is still adapting to the disequilibrium caused in the late Miocene by the uplift of Alpine Corsica. Based on a unique set of geological and *in situ* ^{10}Be cosmogenic data, we demonstrate that tectonic uplift pushed the drainage divide, originally located on Variscan Corsica, eastward and generated a linear, fault-controlled valley that hosted the north-flowing Paleo-Ostriconi River. The landscape responded to the uplift via multi-stage river capture, and the divide eventually migrated back to the west to again become largely fixed on the resistant Variscan spine. In this framework, ~1280 km^2 of basin area originally draining towards the Ligurian Sea were abruptly connected, since the Pliocene, to the base level of the capturing Tavignano and Golo rivers. This led to the formation of a large Pliocene-Quaternary submarine fan offshore the Tyrrhenian coast, associated to an increased sediment yield that was three times greater than the average sediment yield in the same source-to-sink system during the

Holocene. Concentrated erosion persists today around long-lived knickpoints that are still moving through the drainage system after millions of years. Our results demonstrate that a full consideration of landscape response times to onshore disturbances is a prerequisite for any reliable interpretation of the offshore sedimentary archive.

CRediT author statement

Marco G. Malusà: Conceptualization, Formal analysis, Investigation, Resources, Writing - Original Draft, Visualization, Funding acquisition. **Alberto Resentini**: Formal analysis, Investigation, Resources, Software, Visualization. **Hella Wittmann:** Formal analysis, Investigation, Project administration, Funding acquisition.

Acknowledgements

Cosmogenic analyses funded by DFG Project WI 3874/3-1 to H.W. and M.M. We thank Stefan Heinze and Steve Binnie from the University of Cologne for performing AMS measurements, Philippe Rossi for the insightful discussions on the geology of Corsica, and two anonymous reviewers for their constructive comments.

References

1. Balco, G., Stone, J.O., Lifton, N.A., Dunai, T.J., 2008. A complete and easily accessible means of calculating surface exposure ages or erosion rates from 10Be and 26Al measurements. Quaternary Geochronology 3, 174-195.
2. Bender, A. M., Lease, R. O., Corbett, L. B., Bierman, P. R., Caffee, M. W., & Rittenour, T. M. (2020). Late Cenozoic climate change paces landscape adjustments to Yukon River capture. Nature Geoscience, 13(8), 571-575.
3. Bowman, D. (2023). Base-level Impact: A Geomorphic Approach. Springer Nature, 154 pp.
4. Bracciali, L., Najman, Y., Parrish, R. R., Akhter, S. H., & Millar, I. (2015). The Brahmaputra tale of tectonics and erosion: Early Miocene river capture in the Eastern Himalaya. Earth and Planetary Science Letters, 415, 25-37.
5. Calcagno, P., Thinon, I., Courrioux, G., Guillen, A., & Guenoc, P. (2004). 3D geometric modelling: A tool for margin and basin interpretation illustrated with the eastern Corse case-study (NW Mediterranean sea). In RST, Joint Earth Sciences Meeting, Société Géologique de France–Geologische Vereinigung, Strasbourg.
6. Calves, G., Toucanne, S., Jouet, G., Charrier, S., Thereau, E., Etoubleau, J., ... & Lericolais, G. (2013). Inferring denudation variations from the sediment record; an example of the last glacial cycle record of the Golo Basin and watershed, East Corsica, western Mediterranean sea. Basin Research, 25(2), 197-218.

7. Caron, J. M., Loÿe-Pilot, M. D., Dominici, R., Scius, H., & Vautrelle, C. (1990). Notice explicative, Carte géologique de la France (1: 50 000), feuille Pietra di Verde, n∘ 1115. Bureau de Recherches Géologiques et Minières Orléans.
8. Castillo, M., Ferrari, L., & Muñoz-Salinas, E. (2017). Knickpoint retreat and landscape evolution of the Amatlán de Cañas half-graben (northern sector of Jalisco Block, western Mexico). Journal of South American Earth Sciences, 77, 108-122.
9. Contrucci, I., Nercessian, A., Béthoux, N., Mauffret, A., & Pascal, G. (2001). A Ligurian (western Mediterranean Sea) geophysical transect revisited. Geophysical Journal International, 146(1), 74-97.
10. Cubells, J. F., Ferrandini, J., Maurel-Ferrandini, M., Gaudant, J., & Loÿe-Pilot, M. D. (1994). Présence du genre Aphanius Nardo, famille des Cyprinodontidae, dans le Miocène du bassin de Francardo-Ponte Leccia (Corse). Géologie méditerranéenne, 21(1), 19-24.
11. Danišík, M., Kuhlemann, J., Dunkl, I., Székely, B., & Frisch, W. (2007). Burial and exhumation of Corsica (France) in the light of fission track data. Tectonics, 26(1).
12. Danišík, M., Kuhlemann, J., Dunkl, I., Evans, N. J., Székely, B., & Frisch, W. (2012). Survival of ancient landforms in a collisional setting as revealed by combined fission track and (U-Th)/He thermochronometry: A case study from Corsica (France). The Journal of Geology, 120(2), 155-173.
13. Dewald, A., Heinze, S., Jolie, J., Zilges, A., Dunai, T., Rethemeyer, J., Melles, M., Staubwasser, M., Kuczewski, B., Richter, J., Radtke, U., von Blanckenburg, F., Klein, M., 2013. CologneAMS, a dedicated center for accelerator mass spectrometry in Germany. Nuclear Instruments and Methods in Physics Research Section B: Beam Interactions with Materials and Atoms 294, 18-23.
14. Dunne, J., Elmore, D., Muzikar, P., 1999. Scaling factors for the rates of production of cosmogenic nuclides for geometric shielding and attenuation at depth on sloped surfaces. Geomorphology 27, 3-11.
15. Faccenna, C., Becker, T. W., Lucente, F. P., Jolivet, L., & Rossetti, F. (2001). History of subduction and back arc extension in the Central Mediterranean. Geophysical Journal International, 145(3), 809-820.
16. Fellin, M. G., Zattin, M., Picotti, V., Reiners, P. W., & Nicolescu, S. (2005). Relief evolution in northern Corsica (western Mediterranean): Constraints on uplift and erosion on long-term and short-term timescales. Journal of Geophysical Research: Earth Surface, 110(F1).
17. Ferrandini, J., Rossi, P., Ferrandini, M., Farjanel, G., Ginsburg, L., Schuler, M., & Geissert, F. (1999). La formation conglomératique du Vazzio près d'Ajaccio (Corse-du-Sud), un témoin des dépôts du Chattien supérieur continental synrift en Méditerranée occidentale. Comptes Rendus de l'Académie des Sciences-Series IIA-Earth and Planetary Science, 329(4), 271-278.
18. Forzoni, A., Storms, J. E. A., Reimann, T., Moreau, J., & Jouet, G. (2015). Non-linear response of the Golo River system, Corsica, France, to Late Quaternary climatic and sea level variations. Quaternary Science Reviews, 121, 11-27.
19. Gallen, S. F. (2018). Lithologic controls on landscape dynamics and aquatic species evolution in post-orogenic mountains. Earth and Planetary Science Letters, 493, 150-160.
20. Gervais, A., Savoye, B., Piper, D. J., Mulder, T., Cremer, M., & Pichevin, L. (2004). Present morphology and depositional architecture of a sandy confined submarine system:

the Golo turbidite system (eastern margin of Corsica). Geological Society, London, Special Publications, 222(1), 59-89.

21. Gradstein, F. M., Ogg, J. G., & Smith, A. G. (Eds.). (2004). A geologic time scale 2004 (Vol. 86). Cambridge University Press.
22. Granger, D. E., Kirchner, J. W., & Finkel, R. (1996). Spatially averaged long-term erosion rates measured from in situ-produced cosmogenic nuclides in alluvial sediment. The Journal of Geology, 104(3), 249-257.
23. Jauzein A., M.-D Pilot, F Orszag-Sperber (1976) Notice explicative, Carte géologique de la France (1: 50 000), feuille Ghisonaccia, n∘ 1119. Bureau de Recherches Géologiques et Minières Orléans.
24. Kuhlemann, J., van der Borg, K., Bons, P. D., Danišík, M., & Frisch, W. (2008). Erosion rates on subalpine paleosurfaces in the western Mediterranean by in-situ 10Be concentrations in granites: implications for surface processes and long-term landscape evolution in Corsica (France). International Journal of Earth Sciences, 97(3), 549-564.
25. Lahondère, J.C., Conchon, O., Lahondère D., Dominici, R., Vautrelle, C. (1994). Notice explicative, Carte géologique de la France (1: 50 000), feuille Vescovato, n∘ 1107. Bureau de Recherches Géologiques et Minières Orléans.
26. Lal, D., 1991. Cosmic ray labeling of erosion surfaces: in situ nuclide production rates and erosion models. Earth and Planetary Science Letters 104, 424-439.
27. Loget, N., & Van Den Driessche, J. (2009). Wave train model for knickpoint migration. Geomorphology, 106(3-4), 376-382.
28. Loÿe-Pilot, M. D., Durand-Delga, M., Feinberg, H., Gourinard, Y., & Magné, J. (2004). Les formations burdigaliennes de Corse orientale dans leur cadre géodynamique. Comptes Rendus Géoscience, 336(10), 919-930.
29. Malusà, M. G., Faccenna, C., Baldwin, S. L., Fitzgerald, P. G., Rossetti, F., Balestrieri, M. L., Ellero, A., Ottria, G., & Piromallo, C. (2015). Contrasting styles of (U) HP rock exhumation along the Cenozoic Adria-Europe plate boundary (Western Alps, Calabria, Corsica). Geochemistry, Geophysics, Geosystems, 16(6), 1786-1824.
30. Malusà, M. G., Danišík, M., & Kuhlemann, J. (2016). Tracking the Adriatic-slab travel beneath the Tethyan margin of Corsica–Sardinia by low-temperature thermochronometry. Gondwana Research, 31, 135-149.
31. Manger, G.E. (1963). Porosity and bulk density of sedimentary rocks. Geological Survey Bulletin 1144-E.
32. Mauffret, A., Contrucci, I., & Brunet, C. (1999). Structural evolution of the Northern Tyrrhenian Sea from new seismic data. Marine and Petroleum Geology, 16(5), 381-407.
33. Molliex, S., Jouet, G., Freslon, N., Bourles, D. L., Authemayou, C., Moreau, J., & Rabineau, M. (2017). Controls on Holocene denudation rates in mountainous environments under Mediterranean climate. Earth Surface Processes and Landforms, 42(2), 272-289.
34. Molliex, S., Jouet, G., Blard, P. H., Moreau, J., Demartini, J., Storms, J. E., ... & Team, A. (2021). Quaternary evolution of the Golo river alluvial plain (NE Corsica, France). Quaternary Geochronology, 61, 101115.
35. Perron, J. T., & Royden, L. (2013). An integral approach to bedrock river profile analysis. Earth surface processes and landforms, 38(6), 570-576.
36. Rollet, N., Déverchère, J., Beslier, M. O., Guennoc, P., Réhault, J. P., Sosson, M., & Truffert, C. (2002). Back arc extension, tectonic inheritance, and volcanism in the Ligurian Sea, Western Mediterranean. Tectonics, 21(3), 6-1.

37. Rossetti, F., Glodny, J., Theye, T., & Maggi, M. (2015). Pressure–temperature–deformation–time of the ductile Alpine shearing in Corsica: From orogenic construction to collapse. Lithos, 218, 99-116.
38. Rossi, P., & Cocherie, A. (1991). Genesis of a Variscan batholith: Field, petrological and mineralogical evidence from the Corsica-Sardinia batholith. Tectonophysics, 195(2-4), 319-346.
39. Rossi, P., Lahondère, J.C., Lluch, D., Loye-Pilot, M.D., & Jaquet, M. (1994). Notice explicative, Carte Géologique de la France (1: 50.000) feuille Saint Florent, n∘ 1103, Bureau de Recherches Géologiques et Minières Orléans. Notice explicative, BRGM, Orléans, 93.
40. Rossi, P., Oggiano, G., & Cocherie, A. (2009). A restored section of the "southern Variscan realm" across the Corsica–Sardinia microcontinent. Comptes rendus géoscience, 341(2-3), 224-238.
41. Shugar, D. H., Clague, J. J., Best, J. L., Schoof, C., Willis, M. J., Copland, L., & Roe, G. H. (2017). River piracy and drainage basin reorganization led by climate-driven glacier retreat. Nature Geoscience, 10(5), 370-375.
42. Schwanghart, W., Scherler, D., 2014. Short Communication: TopoToolbox 2 – MATLAB-based software for topographic analysis and modeling in Earth surface sciences. Earth Surface Dynamics 2, 1-7.
43. Schwanghart, W., & Scherler, D. (2017). Bumps in river profiles: uncertainty assessment and smoothing using quantile regression techniques. Earth Surface Dynamics, 5(4), 821-839.
44. Serrano, O., Allanic, C., & Magar, M. (2013). Synthèse Géologique du Bassin Tertiaire de la Plaine Orientale Corse—Liaison Terre-Mer Entre San Nicolao et Solenzara, p. 181. BRGM report RP62303FR.
45. Sømme, T. O., Piper, D. J., Deptuck, M. E., & Helland-Hansen, W. (2011). Linking onshore–offshore sediment dispersal in the Golo source-to-sink system (Corsica, France) during the late Quaternary. Journal of Sedimentary Research, 81(2), 118-137.
46. Sweet, M. L., Gaillot, G. T., Jouet, G., Rittenour, T. M., Toucanne, S., Marsset, T., & Blum, M. D. (2020). Sediment routing from shelf to basin floor in the Quaternary Golo System of Eastern Corsica, France, western Mediterranean Sea. Bulletin, 132(5-6), 1217-1234.
47. Thinon, I., Guennoc, P., Serrano, O., Maillard, A., Lasseur, E., & Rehault, J. P. (2016). Seismic markers of the Messinian Salinity Crisis in an intermediate-depth basin: Data for understanding the Neogene evolution of the Corsica Basin (northern Tyrrhenian Sea). Marine and Petroleum Geology, 77, 1274-1296.
48. von Blanckenburg, F., 2005. The control mechanisms of erosion and weathering at basin scale from cosmogenic nuclides in river sediment. Earth and Planetary Science Letters 237, 462-479.
49. von Blanckenburg, F., Hewawasam, T., Kubik, P.W., 2004. Cosmogenic nuclide evidence for low weathering and denudation in the wet, tropical highlands of Sri Lanka. Journal of Geophysical Research-Earth Surface 109.
50. Walford, H. L., White, N. J., & Sydow, J. C. (2005). Solid sediment load history of the Zambezi Delta. Earth and Planetary Science Letters, 238(1-2), 49-63.
51. Weissel, J. K., & Seidl, M. A. (1997). Influence of rock strength properties on escarpment retreat across passive continental margins. Geology, 25(7), 631-634.

52. Zarki-Jakni, B., van der Beek, P., Poupeau, G., Sosson, M., Labrin, E., Rossi, P., & Ferrandini, J. (2004). Cenozoic denudation of Corsica in response to Ligurian and Tyrrhenian extension: Results from apatite fission track thermochronology. Tectonics, 23(1).
53. Zheng, H., Clift, P. D., Wang, P., Tada, R., Jia, J., He, M., & Jourdan, F. (2013). Pre-miocene birth of the Yangtze River. Proceedings of the National Academy of Sciences, 110(19), 7556-7561.

Figure 1

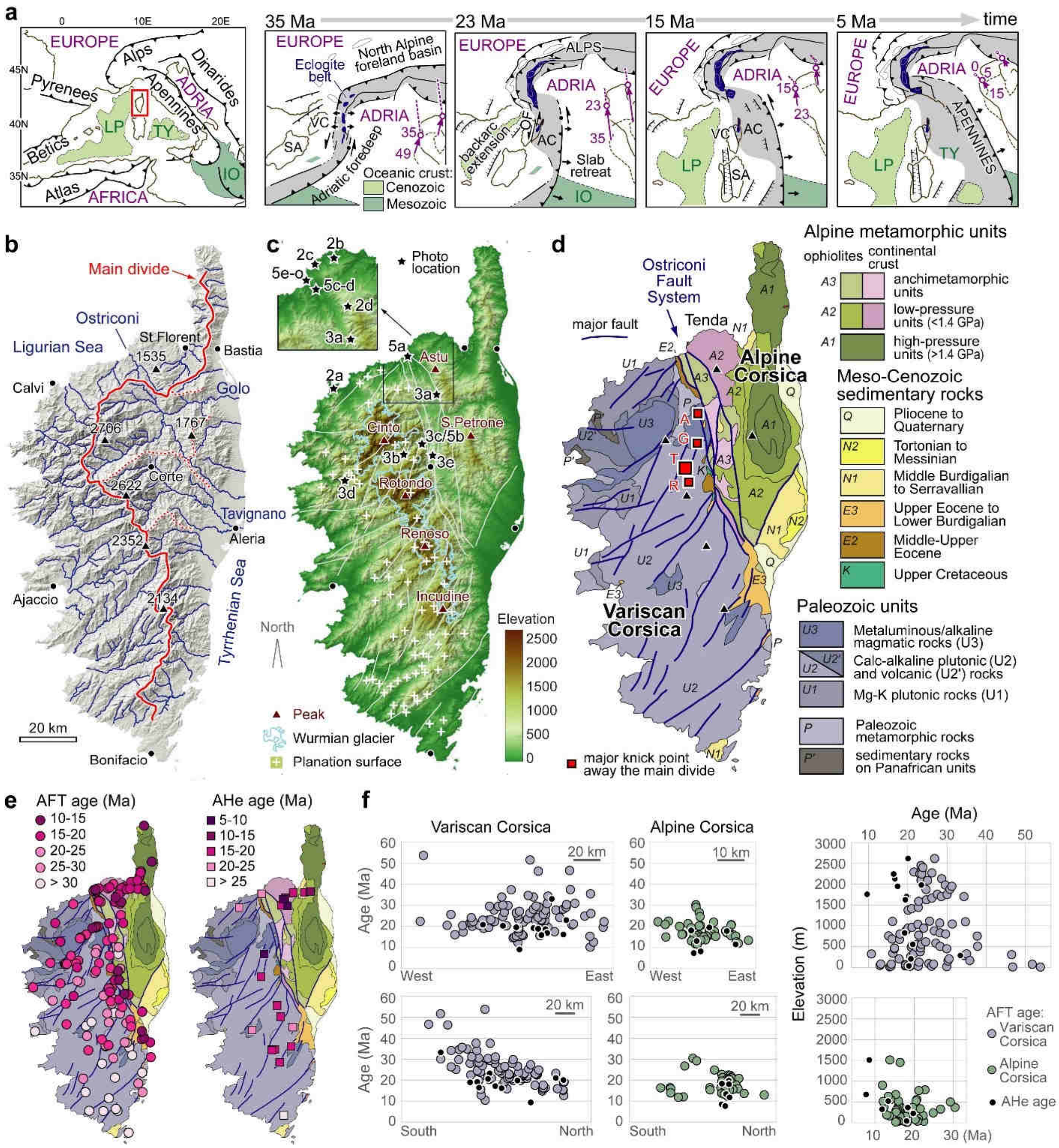

Figure 1: Geologic setting of Corsica. a: Tectonic sketch map of the Western Mediterranean and Cenozoic evolution of the Adria-Europe plate boundary in four steps (after Malusà et al. 2015). The red box indicates the location of frames (b) to (e). The purple arrows show relative Adria-Europe plate motion (numbers are ages in Ma). Acronyms: AC, Alpine Corsica; IO, Ionian; LP, Ligurian-Provençal; OF, Ostriconi fault system; TY, Tyrrhenian; SA, Sardinia; VC, Variscan Corsica. **b:** Shaded-relief map and associated river network (in blue). Thick red line = main drainage divide. Dashed red line = boundary of the Golo and Tavignano rivers catchments.

Numbers in black = elevation (m a.s.l.) of the main peaks indicated in (c). **c:** Elevation map showing the major planation surfaces of Variscan Corsica (white crosses, Danišík et al. 2012) and the distribution of glaciers during the Wurmian maximum (Kuhlemann et al. 2008). Stars indicate the location of pictures shown in Figs. 2, 4 and 5. White lines = main faults shown in (d). **d:** Geologic map simplified after Malusà et al. (2016). The red squares indicate the major knickpoints of Fig. 4 (A=Asco; G=Golo; R=Restonica; T=Tavignano). **e:** Compilation of apatite fission-track (AFT) and (U-Th)/He (AHe) ages (after Zarki-Jakni et al., 2004; Fellin et al., 2005; Danišík et al., 2007; 2012). **f:** E-W, N-S, and elevation distribution of AFT and AHe ages in Variscan and Alpine Corsica.

684 Figure 2

685

686 **Figure 2: Post-Oligocene rock uplift recorded by marine terraces. a:** Marine terraces (marked
687 by arrows) in plutonic rocks of Variscan Corsica (U1 in Fig. 1d) exposed south of Calvi. **b:** Marine
688 terraces (marked by arrows) in Tenda Unit metasediments, Alpine Corsica (A2 in Fig. 1d) located
689 at elevations between 350 and 400 m a.s.l. (Agriates Desert locality). **c:** Raised beach with typical
690 swash cross stratification preserved at ~40 m a.s.l. on top of the Tenda Unit paragneisses (Punta
691 di l'Acciolu locality). Similar deposits on Tenda Unit rocks are documented at elevations as high
692 as 95 m (Monticellacciu locality). **d:** Series of elevated stepped marine terraces in Tenda Unit
693 metagranitoids (A2 in Fig. 1d) on the right slope of the Ostriconi Valley, at elevations between
694 500 and 1000 m a.s.l. (Monte a Lecchia locality). Picture locations in Fig. 1c.

Figure 3

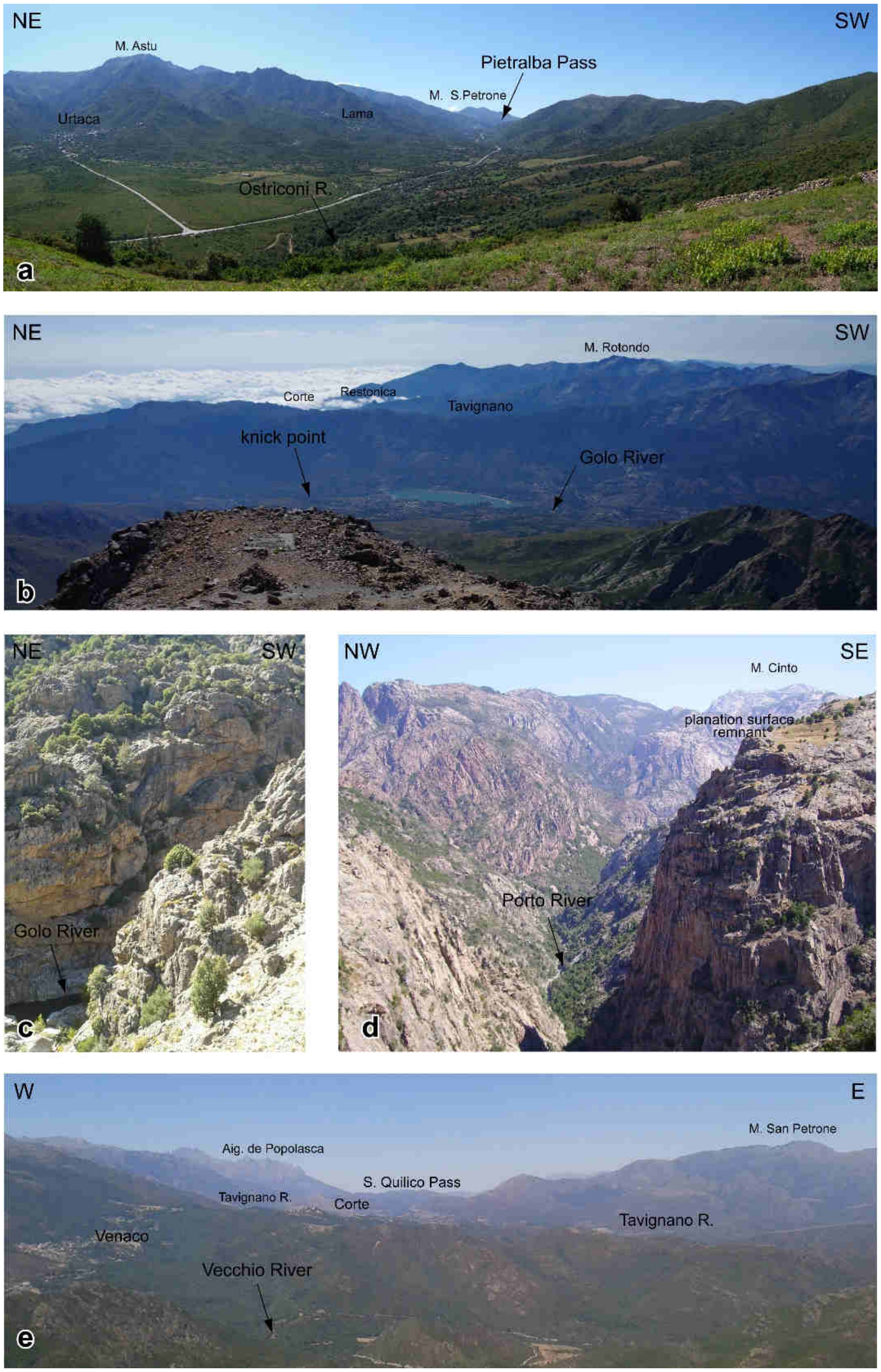

Figure 3: Field geomorphologic evidence of river capture. a: View of the beheaded valley of the Ostriconi River, which has lost the upper part of its catchment beyond the Pietralba Pass. The valley is carved along the Ostriconi Fault, which juxtaposes to the SW the very-low-grade ophiolites and (meta)sedimentary rocks of the Balagne Nappe, and to the NE the metagranitoids

and paragneisses of the Tenda Unit. On the left side of the photo is the alluvial fan of Urtaca, made up of boulders of metagranitoids and paragneisses of the Tenda Unit. Behind the Pietralba Pass is Monte S. Petrone, consisting of high-pressure metaophiolites of the Castagniccia tectonic dome. The transverse profile of the Ostriconi valley is too large to be related to the modern Ostriconi River, which is evidently underfit (cf. Fig. 4b). **b:** The wide and relatively flat upper Golo valley seen from the summit of Monte Cinto. The arrow downstream the Calacuccia artificial lake indicates the major knickpoint marked by a red square in Fig. 4a. Lithologies are the same before and after the knickpoint. In the background are the upper Tavignano and Restonica valleys, also showing a major knickpoint away from the main divide (Fig. 4a). Alpine Corsica is in the background below the clouds due to its lower elevation compared to Variscan Corsica. **c:** Steepened valley walls in the upper Golo valley, downstream the knickpoint shown in (b). **d:** View of the Porto River showing steep walls cutting old planation surfaces, but no major knickpoints far from the main divide. Lithologies are the same as in the upper Golo valley. **e:** Upper part of the Tavignano drainage interpreted as previously belonging to the Paleo-Ostriconi River catchment. The San Quilico Pass, in the background, was originally located along the Paleo-Ostriconi valley floor, which was carved in correspondence of the Ostriconi Fault. Here the fault juxtaposes the Variscan basement, to the W, and the high-pressure metaophiolites of the Castagniccia tectonic dome to the E (Monte S. Petrone). See picture locations in Fig. 1c.

Figure 4

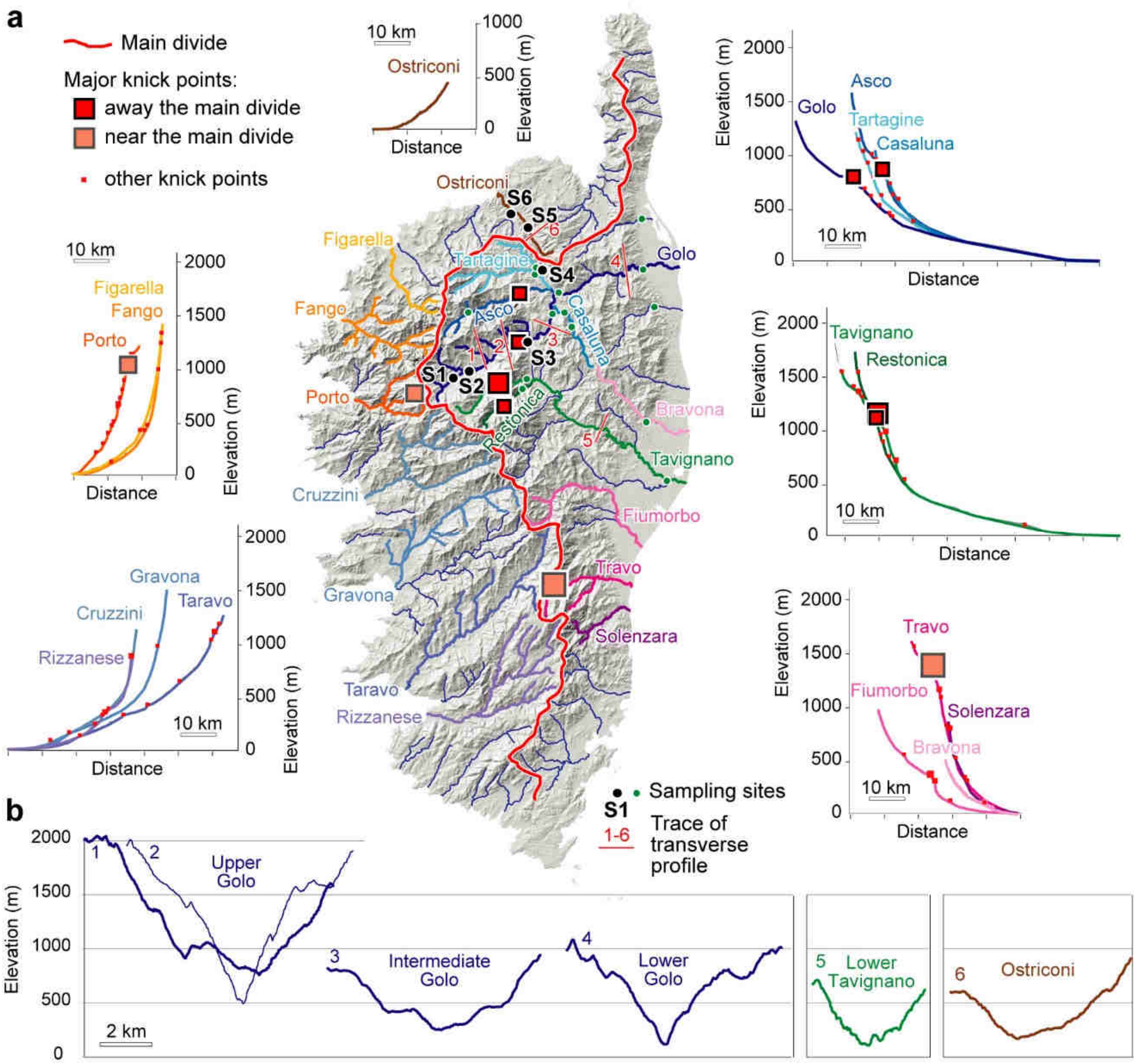

Figure 4: River profiles, major knickpoints and sampling sites for cosmogenic ^{10}Be analyses. a: The longitudinal profiles of the Restonica, Tavignano, upper Golo and Asco rivers, flowing into the Tyrrhenian Sea (on the right), reveal major knickpoints away the main divide (dark red squares) that are not observed along rivers that flow into the Ligurian Sea (on the left). Black dots in the map indicate sampling sites for cosmogenic ^{10}Be analyses (S1 to S6, this work), smaller green dots indicate samples analyzed by Molliex et al. (2017). **b:** Transverse profiles (see (a) for locations) highlight wider valleys for the Ostriconi and upper and intermediate Golo compared to the narrower valleys of the lower Golo and Tavignano.

Figure 5

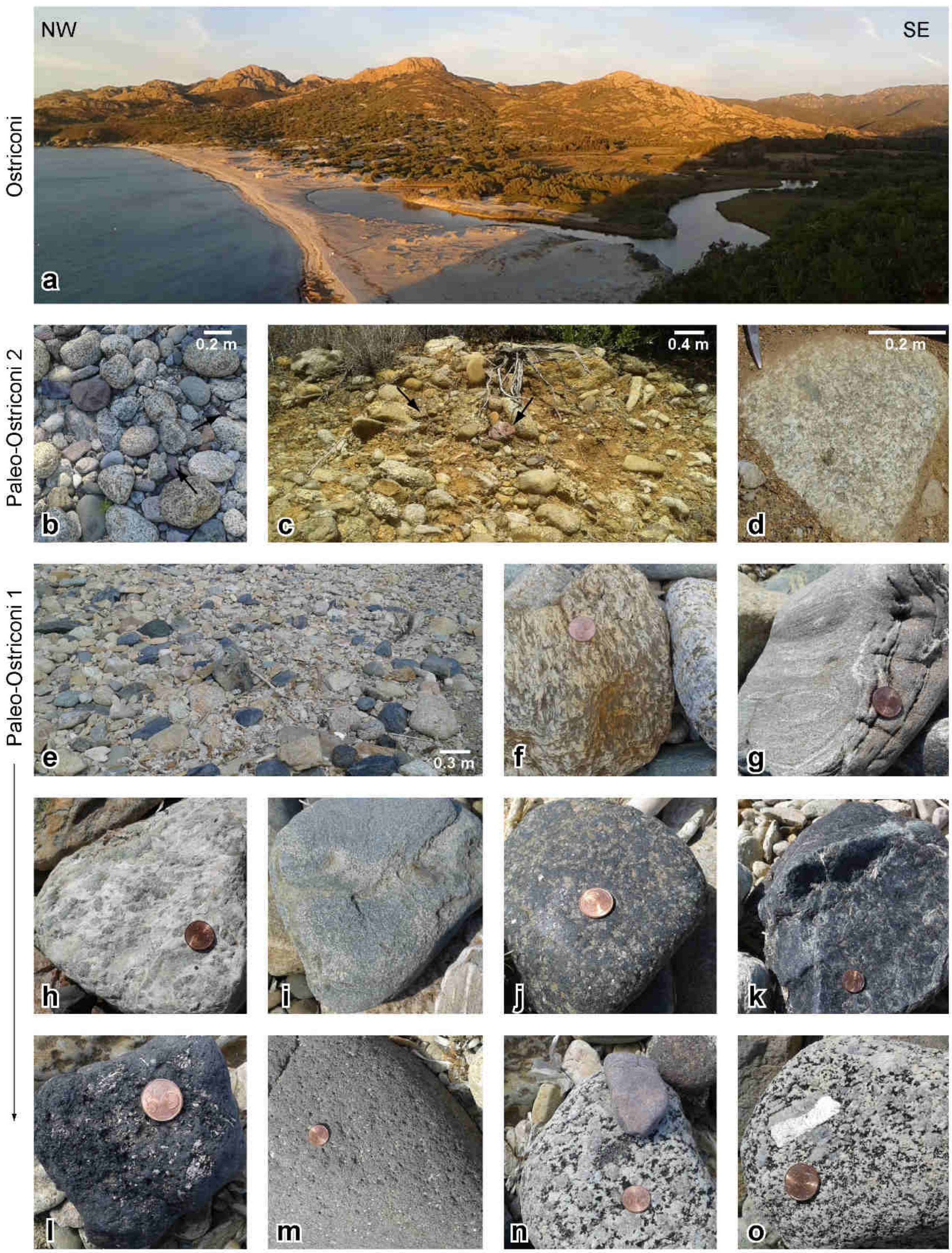

Figure 5: Field sedimentology evidence of river capture. **a:** Fine-grained sediments and associated low-energy depositional environments at the mouth of the modern Ostriconi River. **b:** Modern sediments of the upper Golo River including cobbles of monzonite, quartz-monzonite,

andesite (U2 magmatic suite *sensu* Rossi and Cocherie 1991) and smaller cobbles of reddish rhyolite (marked by arrows) of the ancient Monte Cinto caldera (U3 magmatic suite *sensu* Rossi and Cocherie 1991). **c, d:** Outcrop of ancient fluvial sediments of the *"Paleo-Ostriconi 2"* stage (Ogliastro locality) composed of metagranitoids and paragneisses of the Tenda Unit but also including cobbles of quartz-monzonite (see close-up view in (d)), andesite with plagioclase phenocrysts, and Monte Cinto rhyolite (marked by arrows in (c)) not exposed today in the modern Ostriconi river catchment. **e:** Pebbly beach of reworked deposits of the *"Paleo-Ostriconi 1"* stage (Anse de Peraiola locality) including abundant pebbles derived from high-pressure metaophiolitic units of Alpine Corsica (see frames (g) to (k)) and pebbles derived from U2-U3 magmatic suites of Variscan Corsica (see frames (l) to (o)), which are not exposed today in the modern Ostriconi river catchment. Close-ups: **f:** metagranitoid of the Tenda Unit. **g:** high-pressure calcschist. **h:** metagabbro; **i:** greenschist. **j:** ultramafics (peridotite/pyroxenite). **k:** serpentinite. **l:** vesiculated basalt (U3 suite). **m:** vesiculated andesite with plagioclase phenocrysts (U2 suite); **n:** monzonite with K-feldspar phenocrysts (U2 suite) and Monte Cinto reddish rhyolite (U3 suite). **o:** quartz-monzonite (U2 suite). Remnants of coarse-grained Paleo-Ostriconi fluvial deposits are also found on the mountains in the background of picture (a), at elevations as high as 110 m a.s.l., and include boulders of U2 quartz-monzonite and U3 rhyolite (Monticellacciu and Cima Forca localities). See picture locations in Fig. 1c.

Figure 6

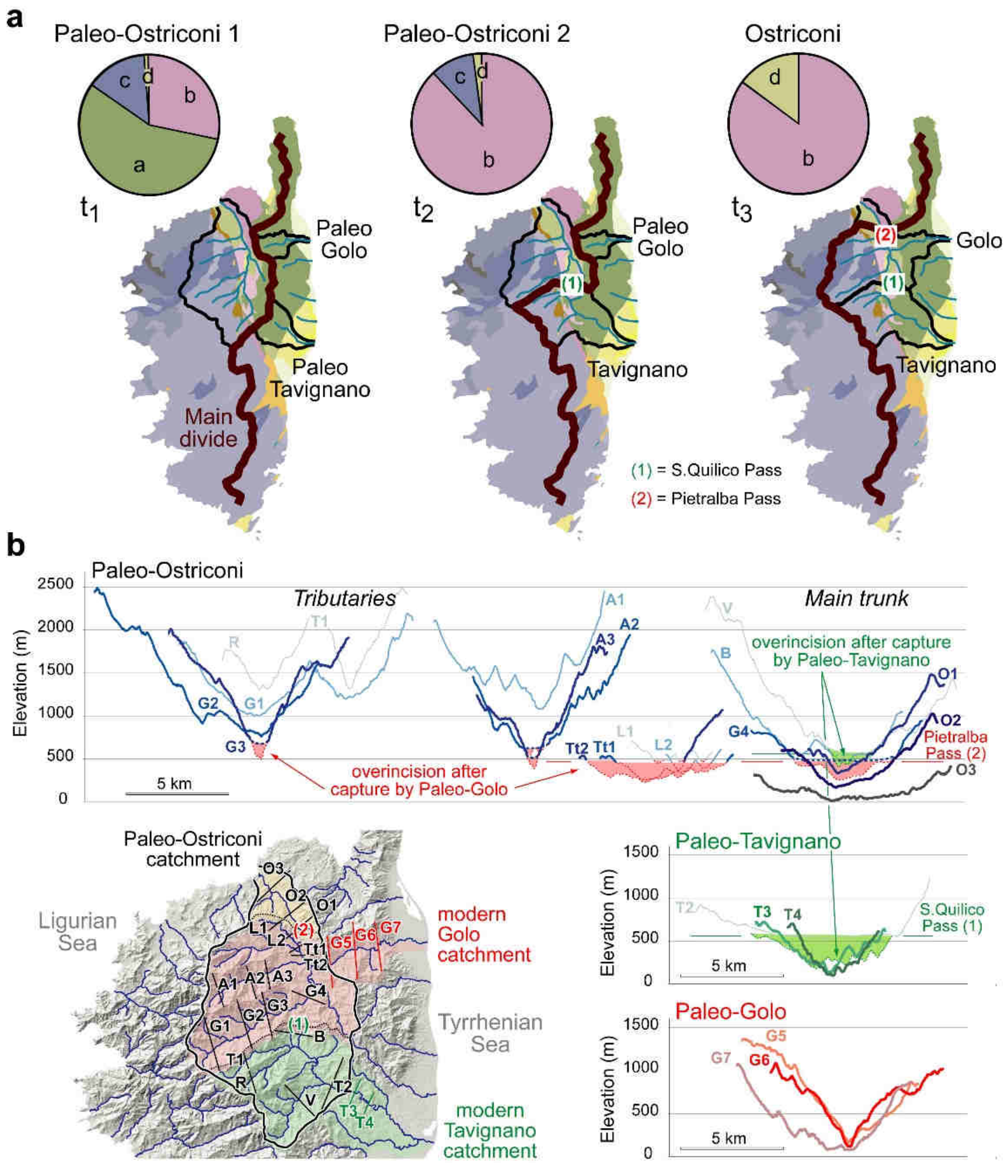

Figure 6: Changes in modal compositions and overincision during progressive river capture. **a:** Inferred Paleo-Ostriconi 1 (t_1) and Paleo-Ostriconi 2 (t_2) paleodrainages, and modal compositions of associated pebbly deposits (pie charts) compared to the modern Ostriconi River (t_3). Pebble derivation: a, dark green = Castagniccia metaophiolites; b, pink = Alpine continental metamorphic rocks (e.g., Tenda Unit); c, violet = Paleozoic units of Variscan Corsica; d, light green = Alpine very-low-grade metasediments (Balagne Nappe). The black lines in the map indicate drainage boundaries, the thick brown line indicates the position of the main divide. **b:** Transverse profiles of modern rivers rearranged according to their position in the inferred Paleo-Ostriconi 1 drainage network. The Pietralba and S. Quilico passes, located along the original Paleo-Ostriconi valley floor, provide lower-bound constraints to the amount of overincision after capture by Paleo-Tavignano (> 400 m overincision, in green) and Paleo-Golo (> 250 m overincision, in red). Profiles acronyms: A1-A3 = Asco; B = Bistuglio; G1-G7 = Golo; L1-L2 = Lagani; O1-O3 = Ostriconi; R = Restonica; T1-T4 = Tavignano; Tt1-Tt2 = Tartagnine; V = Vecchio.

Figure 7

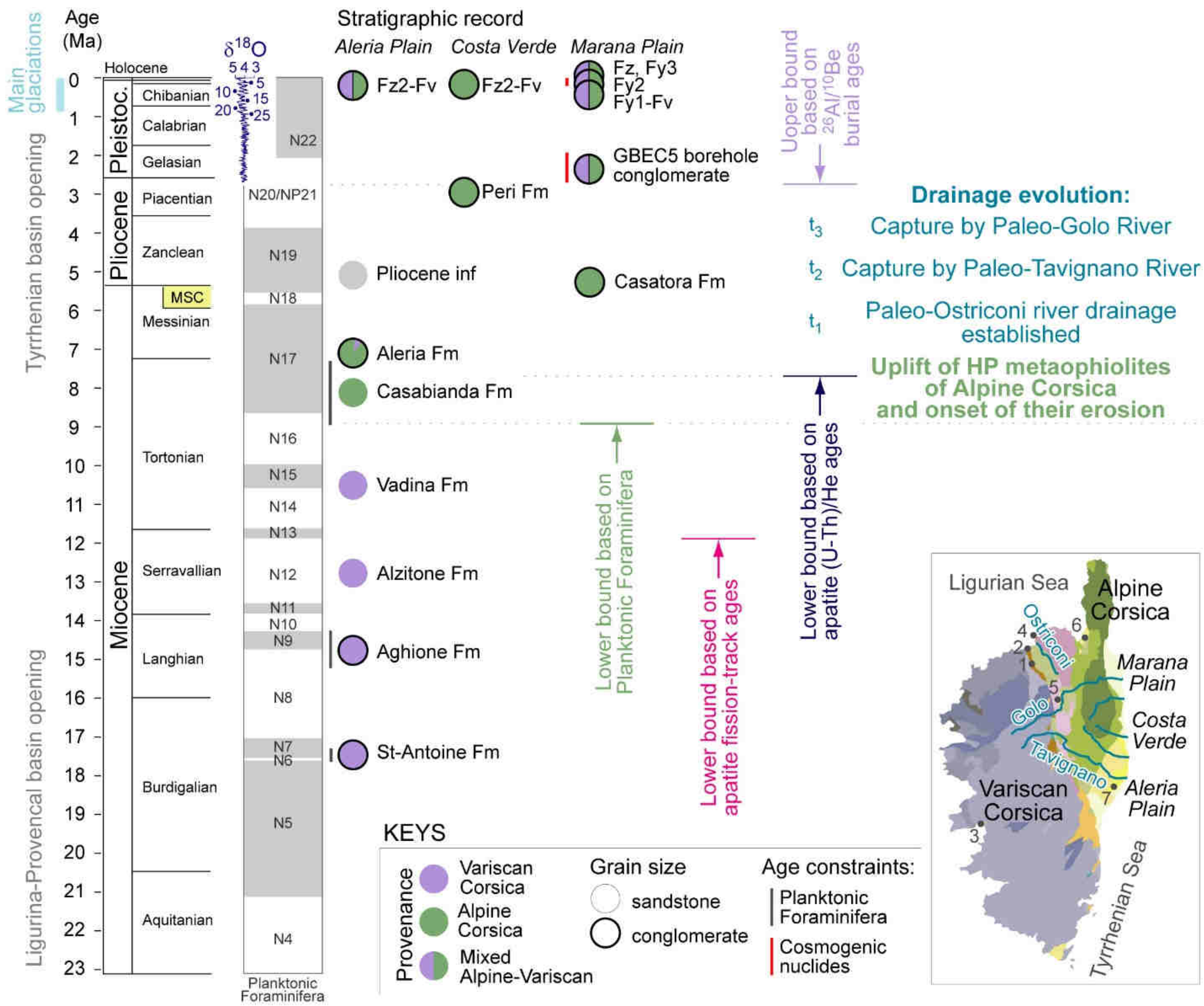

Figure 7: Time constraints provided by sediment modal composition and low-temperature thermochronology. Biostratigraphic ages and provenance information for the Miocene-to-Holocene formations of the Aleria Plain, Costa Verde and Marana Plain (see inset for locations) indicate an evolution of the Paleo-Ostriconi river drainage bracketed between the late Tortonian and the Pliocene (data after Jauzein et al. 1976; Caron et al. 1990; Lahondère et al., 1994; Loÿe-Pilot et al. 2004; Serrano et al. 2013). Provenance data for the Pleistocene-Holocene formations of the Marana Plain and cosmogenic data for the borehole GBEC5-2 conglomerate are after Molliex et al. (2021). Apatite fission track and (U-Th)/He age constraints same as in Fig. 1. Neogene time scale, composite marine $\delta^{18}O$ isotope sequence (in blue), and planktonic foraminifera zonation after Gradstein et al. (2004). MSC= Messinian Salinity Crisis. Numbers in the map indicate successions described in Sect. 4.4 (1 = Palasca; 2 = Lozari; 3 = Vazzio; 4 = Punta di l'Acciolu; 5 = Francardo-Ponte Leccia; 6 = St-Florent; 7 = Aleria).

Figure 8

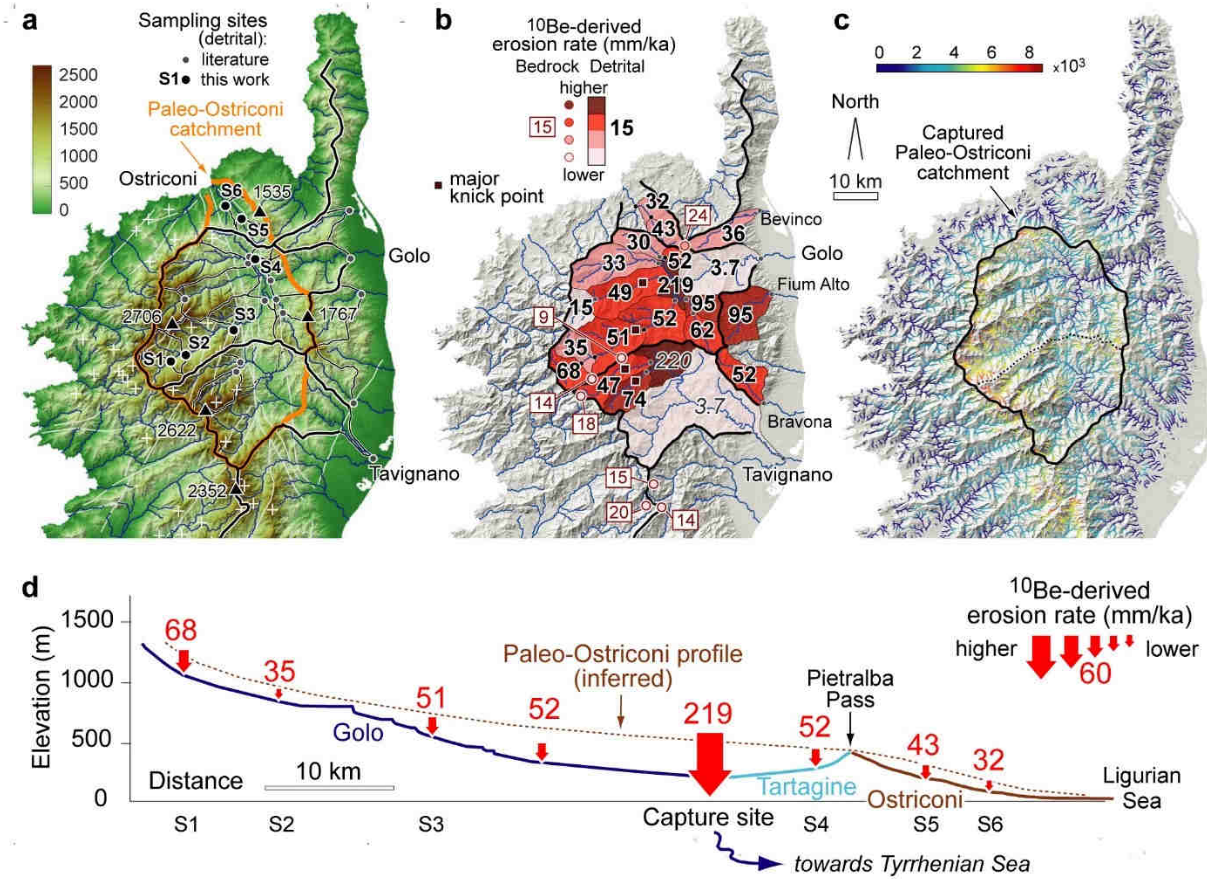

Figure 8: Holocene erosion pattern by cosmogenic ^{10}Be data. a: Elevation map of the Paleo-Ostriconi river catchment and locations of detrital samples analyzed for cosmogenic ^{10}Be (the smaller grey dots indicate samples analyzed by Molliex et al. 2017). **b:** Map of ^{10}Be-derived erosion rates (mm/ka, numbers in bold) with rates for nested catchments computed according to the approach of Granger et al. (1996) (see Supplementary Table S3). Values in italics assume similar erosion rates in the lower Golo valley (measured) and the lower Tavignano valley (inferred). Numbers in brown are denudation rates from ^{10}Be concentrations in granites of high-elevation paleosurfaces (Kuhlemann et al. 2008). **c:** Chi-map of northern Corsica. The higher chi-values in the captured Paleo-Ostriconi catchment, as compared to the nearby catchments, indicate a transient landscape with the drainage divide moving toward high-chi headwaters. **d:** Reconstruction of the Paleo-Ostriconi 2 river profile and associated ^{10}Be-derived erosion rates. Note the highest erosion rates still observed in correspondence of the capture site. River color code as in Fig. 4.

Figure 9

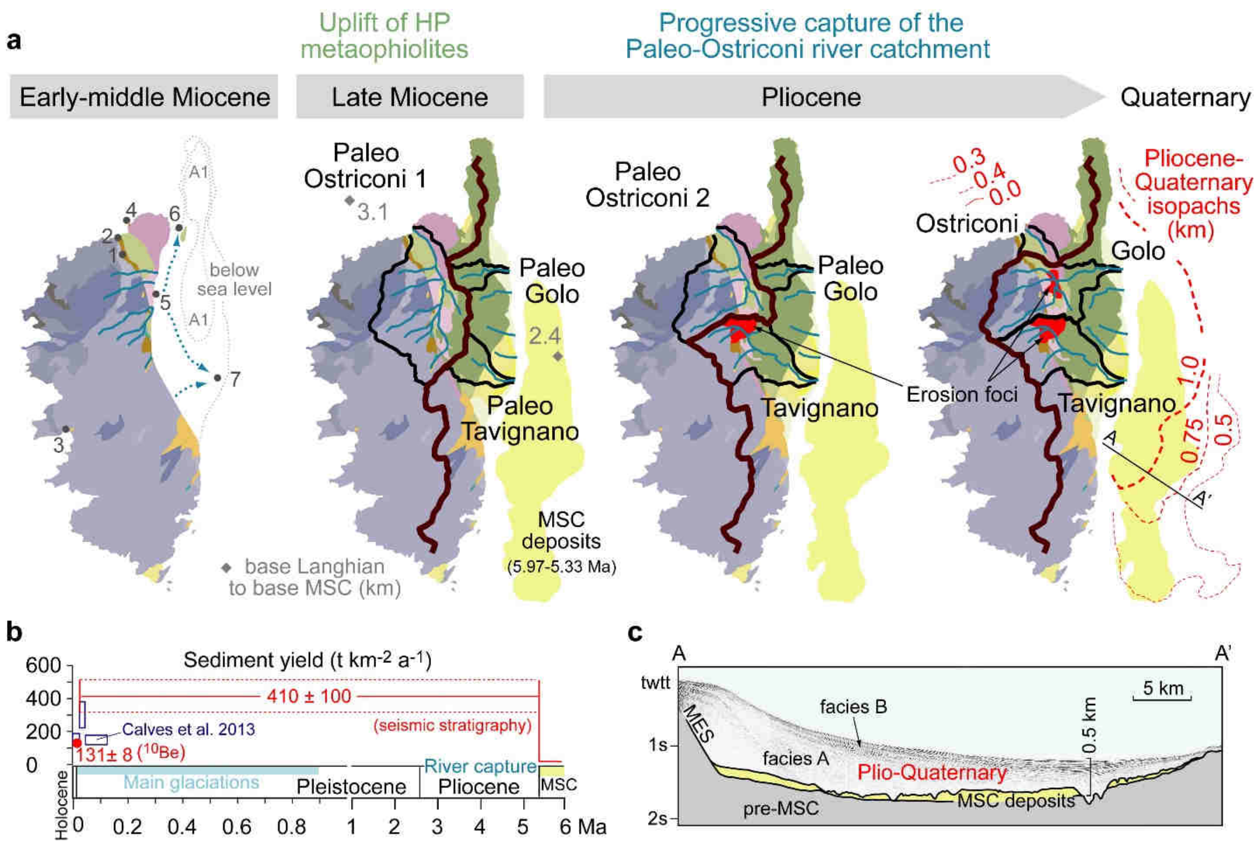

Figure 9: Impact of river capture on offshore sedimentation. a: Post-Oligocene drainage evolution and offshore sedimentation in four steps. The thick brown line indicates the location of the main drainage divide. Offshore deposits related to the Messinian salinity crisis (MSC, yellow area) after Thinon et al. (2016). Pliocene-Quaternary isopachs (km, in red) after Contrucci et al. (2001) for the Ligurian side (as inferred from the LISA01 profile) and Calcagno et al. (2004) for the Tyrrhenian side (as reported in Thinon et al. 2016) using a seismic velocity of 2.0 km s^{-1} for time-to-depth conversion. Base Langhian to base MSC sediment thickness (km, in grey) after Contrucci et al. (2001) (LISA01) for the Ligurian side and Mauffret et al. (1999) (LISA10-W) for the Tyrrhenian side using a seismic velocity of 4.4 km s^{-1} for time-to-depth conversion. Onshore Holocene erosion foci (in red) as in Fig. 8b. Numbers in the early-middle Miocene map as in Fig. 7. **b:** Sediment yield from the Golo and Tavignano catchments as constrained by: (i) ^{10}Be data for the Holocene (131±8 $t\cdot km^{-2}\cdot a^{-1}$, this work); (ii) analysis of the sedimentary record for the last 130 ka (blue empty boxes, after Calves et al. 2013); (iii) seismic stratigraphy for the Pliocene-Pleistocene (410±100 $t\cdot km^{-2}\cdot a^{-1}$, red bar, this work; the error bar includes uncertainties due to time-to-depth conversion and porosity decay). The major increase in sediment yield after the MSC is coeval with capture of the Paleo-Ostriconi catchment. **c:** Cross-section of the Plio-Quaternary submarine fan fed by the Tavignano and Golo rivers (seismic profile BS97-22 modified after Thinon et al. 2016), see location in (a). The surfaces bounding the MSC deposits (in yellow) join up at the edges of the basin to form a single surface (MES). Seismic reflectors are weaker in the lower part of the fan, corresponding to the early stages of drainage reorganization (facies A), and more evident in the upper part of the fan (facies B).

820 Table1. *In situ* ^{10}Be concentrations and denudation rates.

Sample Lab label (grain size)	River Lat/Long	Quartz weight (g)	*In situ* ^{10}Be concentration ($\times 10^4$ at/g_{QTZ})	P_mu (z=0) (at·g^{-1}·yr^{-1})	P_sp (z=0)	Denudation rate (mm/ka)	Apparent age ($\times 10^3$ a)
S1 - MM1 (500-800)	Golo N 42.307370 E 8.946067	43.43	13.09±0.54	0.1221	13.62	67.6±4.1	12.2
S2 - MM2A (250-500)	Golo N 42.318729 E 8.983192	31.75	17.23±0.90	0.1226	13.90	52.1±3.6	16.1
S2 - MM2B (500-800)	Golo N 42.318729 E 8.983192	41.77	17.75±0.78	0.1226	13.91	50.6±3.2	16.1
S3 - MM3 (500-800)	Golo N 42.373785 E 9.119820	28.77	16.29±0.67	0.1187	12.95	51.6±3.2	16.4
S4 - MM4 (500-800)	S. Maria N 42.518805 E 9.171593	37.62	10.24±0.49	0.0967	7.79	51.8±3.4	16.0
S5 - MM5 (500-800)	Ostriconi N 42.602333 E 9.138909	32.45	11.98±0.59	0.0951	7.53	42.8±2.9	21.3
S6 - MM6 (500-800)	Ostriconi N 42.625068 E 9.100545	25.45	12.56±0.60	0.0913	6.82	37.2±2.4	23.8

821